Received: 3 March 2023 | Revised: 31 October 2023 | Accepted: 22 November 2023

DOI: 10.1002/fuce.202300060

Fuel Cells
From Fundamentals to Systems

RESEARCH ARTICLE

Comparison of a solid oxide cell with nickel/gadolinium-doped ceria fuel electrode during operation with hydrogen/steam and carbon monoxide/carbon dioxide

Cedric Grosselindemann[1] | **Felix Kullmann**[1] | **Tibor Lehnert**[2] | **Oliver Fritz**[1] | **Franz-Martin Fuchs**[3] | **André Weber**[1]

[1]Karlsruhe Institute of Technology (KIT), Institute for Applied Materials – Electrochemical Technologies (IAM-ET), Karlsruhe, Germany

[2]Karlsruhe Institute of Technology (KIT), Laboratory for Electron Microscopy, Karlsruhe, Germany

[3]Kerafol Keramische Folien GmbH and Co. KG, Eschenbach, Germany

Correspondence
Cedric Grosselindemann, Karlsruhe Institute of Technology (KIT), Institute for Applied Materials – Electrochemical Technologies (IAM-ET), Adenauerring 20b, 76131 Karlsruhe, Germany.
Email: cedric.grosselindemann@kit.edu

Funding information
Federal Ministry of Education and Research, Grant/Award Number: BMBF 03HY124C; Helmholtz project "Solar Hydrogen"

Abstract

Solid oxide cells (SOCs) offer the possibility to operate on hydrogen/steam (H_2/H_2O), carbon monoxide/carbon dioxide (CO/CO_2), and mixtures thereof in the fuel cell as well as in the electrolyzer mode. In this study, the electrochemical processes in an electrolyte-supported SOC exhibiting a $La_w\ Sr_x\ Co_y\ Fe_z\ O_{(3-\delta)}$ air electrode and a nickel/gadolinium-doped ceria (Ni/CGO) fuel electrode (FE) were analyzed by electrochemical impedance spectroscopy, and the subsequent impedance data analysis by the distribution of relaxation times for CO/CO_2 fuel mixtures. A physicochemical equivalent circuit model was fitted to the measured

List of Abbreviations: ASC, anode-supported cell; ASR, area-specific resistance; AE, air electrode; CGO, gadolinium-doped ceria; CNLS, complex non-linear least square; CO, carbon monoxide; CO_2, carbon dioxide; IV, current-voltage; dc, direct current.; DRT, distribution of relaxation times; ESC, electrolyte-supported cell; FE, fuel electrode; He, helium; H_2, hydrogen; H_2O, steam; LSCF, $La_w\ Sr_x\ Co_y\ Fe_z\ O_{(3-\delta)}$; Ni, nickel; N_2, nitrogen; O_2, oxygen; OCV, open circuit voltage; RQ, parallel connection of Ohmic resistance and constant-phase element; SEM, scanning electron microscopy; SOC, solid oxide cell; SOEC, solid oxide electrolyzer cell; SOFC, solid oxide fuel cell; 3YSZ, 3 mol.% yttria-stabilized zirconia

Latin Letters: a, exponent describing hydrogen partial pressure dependency of the fuel electrodet's exchange current density / -; b, exponent describing steam partial pressure dependency of the fuel electrodet's exchange current density / -; c, exponent describing carbon monoxide partial pressure dependency of the fuel electrodet's exchange current density / -; d, exponent describing carbon dioxide partial pressure dependency of the fuel electrodet's exchange current density / -; B_{ohm}, cell-specific constant for ohmic resistance / K Ω^{-1} m^{-2}; B_{EL}, cell-specific constant for electrodes / $\Omega\ m^2$; D_i, gas diffusion coefficient of the component i / $m^2\ s^{-1}$; E_{act}, activation energy / J mol^{-1}; F, Faraday constant / As mol^{-1}.; G_{eff}, effective gas diffusion parameter / m^{-1}; j, current density / A m^{-2}; $j_{0,EL}$, exchange current density / A m^{-2}; k_1, k_2, k_3, polynomial coefficients / -; L_{EL}, gas diffusion layer / m; m, exponent describing oxygen partial pressure dependency of the air electrodet's exchange current density / -; p, overall pressure / atm; p_{ref}, reference pressure / atm; p_i, partial pressure of the component i / atm; P_{corr}, conversion factor / Pa atm^{-1}; $\tilde{R}$, universal gas constant / J mol^{-1} K^{-1}; R_{diff}, gas diffusion resistance / $\Omega\ m^2$; R_{pol}, polarization resistance / $\Omega\ m^2$; R_{act}, activation resistance / $\Omega\ m^2$; R_{ohm}, Ohmic resistance / $\Omega\ m^2$; T, temperature / K; U_{OCV}, open circuit voltage / V; U_{cell}, cell voltage / V; z, number of exchanged electrons / -

Greek Letters: α, charge transfer coefficient / -; γ, exponential prefactor / A m^{-2}; δ, concentration of oxygen lattice vacancy / -; η, overpotential / V; Ψ, microstructure parameter / -

Subscripts: act, activation; cell, cell; corr, correction; diff, gas diffusion; eff, effective; EL, electrode; OCV, open circuit voltage; ohm, Ohmic; pol, polarization.

spectra. With the help of the extracted parameters, a zero-dimensional direct current cell model was parametrized to simulate the current-voltage behavior of the cell. This approach, previously implemented for H_2/H_2O fuel mixtures, is extended toward CO/CO_2 fuels. It will be shown that the same model – with adapted parameters for the FE – can be applied. A comparison of measured and simulated current-voltage curves showed an excellent agreement for both fuels and operating modes (solid oxide fuel cell/solid oxide electrolyzer cell). Simulations reveal that there is nearly no performance difference between H_2O and CO_2 electrolysis for the electrolyte-supported cell with Ni/CGO FE in comparison to an anode-supported cell with Ni/yttria-stabilized zirconia FE.

KEYWORDS
zero-dimensional direct current performance model, CO_2 electrolysis, distribution of relaxation times, electrochemical impedance spectroscopy, Ni/CGO fuel electrode, solid oxide fuel cell

1 | INTRODUCTION

Among the various types of fuel cells and electrolyzers [1], only solid oxide cells (SOCs) show a high fuel flexibility and can, next to hydrogen (H_2), operate on carbon monoxide (CO) and reformate/syngas [2–6]. Physicochemical cell models that are able to simulate the cell behavior within a wide range of technically relevant operating conditions are a useful tool to optimize the cell design, evaluate optimum operating strategies, and simulate the cell behavior on stack and system levels [7–11]. On the cell level, the development of an impedance-based zero-dimensional direct current (dc) performance model was demonstrated for electrolyte-supported cells (ESCs) [12, 13], metal-supported cells [14], and anode-supported cells [7, 8, 15]. In the work by Leonide et al., this was developed separately for H_2/steam (H_2/H_2O) and CO/carbon dioxide (CO/CO_2) fuel gas mixtures [7, 15]. There, the operation with CO/CO_2 fuel gas mixtures leads to a significant impact on the electrochemical behavior of the anode-supported cell with Ni/8YSZ fuel electrode (FE) resulting in a higher activation energy of the FE with $E_{act,FE,CO/CO_2} = 118.64\ kJ\ mol^{-1}$ in comparison to $E_{act,FE,H_2/H_2O} = 105.04\ kJ\ mol^{-1}$ [7, 15]. Further, the gas diffusion losses in the 1 mm thick anode substrate are increasing due to the substrate thickness and the low effective gas diffusion coefficients [15]. However, gradients with respect to temperature and gas conversion along the gas channels are not considered and require a multiphysics modeling environment. This is provided in the work by Russner et al. [16] for a two-dimensional gas-channel model based on a finite element method for an anode-supported cell (ASC) and electrolyte-supported cell (ESC) design, which shows the impact of individual loss contributions toward a distribution of temperature in a stack layer operated with reformate gas mixtures. Also, a single-channel model for the electrolysis of CO_2 in a SOC is proposed [17]. In the field, so far the solid oxide electrolysis of CO_2 has been applied in eCOs developed by Haldor Topsoe [18–20] and in the Mars Oxygen In Situ Resource Utilization Experiment [21].

In the frame of this work, we focus on comparing the electrochemistry of an ESC with a nickel/gadolinium-doped ceria (Ni/CGO) FE in H_2/H_2O and CO/CO_2 fuel gas mixtures. The zero-dimensional dc performance model developed and validated for the operation with H_2/H_2O [22] is extended to CO/CO_2 fuel gas mixtures in fuel cell and electrolyzer mode enabling the comparison between both fuel gas mixtures. This study shall furthermore provide a basis for the investigation of Ni/CGO electrodes in reformate, respectively, syngas mixtures [3, 23–26].

2 | EXPERIMENTAL SECTION

2.1 | Modeling

The knowledge of the individual loss mechanisms occurring in the cell is crucial in order to develop a zero-dimensional dc performance model. In the open circuit voltage (OCV) minus losses model the different losses such as ohmic losses η_{ohm}, activation losses at the FE $\eta_{act,FE}$ and the air electrode (AE) $\eta_{act,AE}$ as well as gas diffusion losses at the fuel $\eta_{diff,FE}$ and AE $\eta_{diff,AE}$ are subtracted from the OCV U_{OCV} and lead to the cell voltage U_{cell} in Equation (1). In order to describe the electrochemical loss mechanisms in an OCV minus losses model, generally

valid modeling parameters such as activation energies of the electrodes or microstructural parameters are needed. Considering a SOC with a Ni/CGO FE, this work aims for the parametrization under CO/CO_2 fuel mixtures and comparison to H_2/H_2O operation [22]. The impedance-based parametrization and subsequent zero-dimensional dc performance modeling are described in depth [15, 22]. With the help of knowledge about the individual voltage losses, limiting factors toward the cell performance can be identified [27]. In the following, an overview of the parameters needed for CO/CO_2 operation is given.

$$U_{\text{cell}} = U_{\text{OCV}} - \eta_{\text{ohm}} - \eta_{\text{act,FE}} - \eta_{\text{act,AE}} - \eta_{\text{diff,FE}} - \eta_{\text{diff,AE}} \tag{1}$$

Ohmic losses η_{ohm} can be described by the ohmic law according to Equation (2) with the current density j and the ohmic resistance R_{ohm}. The temperature T dependency of the latter is usually expressed by an Arrhenius approach in Equation (3). There, B_{ohm} depicts the cell specific constant for the ohmic resistance, $E_{\text{act,ohm}}$ the ohmic activation energy and $\tilde{R}$ the universal gas constant.

$$\eta_{\text{ohm}} = j \cdot R_{\text{ohm}} \tag{2}$$

$$R_{\text{ohm}}(T) = \frac{T}{B_{\text{ohm}}} \cdot \exp\left(\frac{E_{\text{act,ohm}}}{\tilde{R}T}\right) \tag{3}$$

The Butler-Volmer approach in Equation (4) is suitable in order to determine the activation losses $\eta_{\text{act},EL}$ at the electrodes (EL) caused by the charge transfer reaction with the help of the exchange current density $j_{0,EL}$, the Faraday-constant F, the number of exchanged electrons z and the charge transfer coefficient α_{EL}.

$$j = j_{0,EL}\left[\exp\left(\alpha_{EL}\frac{zF\eta_{\text{act},EL}}{\tilde{R}T}\right) - \exp\left(-(1-\alpha_{EL})\frac{zF\eta_{\text{act},EL}}{\tilde{R}T}\right)\right] \tag{4}$$

For the exchange current density $j_{0,EL}$ knowledge about the partial pressures at the fuel (FE) and air side (AE) in Equations (5) and (6) is necessary with in particular the carbon monoxide partial pressure $p_{\text{CO,FE}}$ and CO_2 partial pressure $p_{\text{CO}_2\text{,FE}}$ as well as the oxygen (O_2) partial pressure $p_{\text{O}_2\text{,AE}}$ at the air side and the reference pressure $p_{\text{ref}} = 1$ atm. In this contribution, all results were generated under atmospheric pressure. Therefore, the impact of the total pressure p can be neglected. In here, $E_{\text{act},EL}$ depicts the activation energy of the fuel and AE, respectively, and γ_{EL} an exponential pre-factor.

$$j_{0,\text{FE}} = \gamma_{\text{FE}}\left(\frac{p_{\text{CO,FE}}}{p_{\text{ref}}}\right)^c\left(\frac{p_{\text{CO}_2\text{,FE}}}{p_{\text{ref}}}\right)^d\exp\left(-\frac{E_{\text{act,FE}}}{\tilde{R}T}\right) \tag{5}$$

$$j_{0,\text{AE}} = \gamma_{\text{AE}}\left(\frac{p_{\text{O}_2\text{,AE}}}{p_{\text{ref}}}\right)^m\exp\left(-\frac{E_{\text{act,AE}}}{\tilde{R}T}\right) \tag{6}$$

The exponential pre-factor γ_{EL} at fuel and air side can be described with Equations (7) and (8), respectively. Here, $B_{\text{FE,CO/CO}_2}$ depicts the cell specific constant for the FE and B_{AE} for the AE.

$$\gamma_{\text{FE}} = \frac{\tilde{R}T}{2FB_{\text{FE,CO/CO}_2}} \cdot \left[\left(\frac{p_{\text{CO,FE}}}{p_{\text{ref}}}\right)^c\left(\frac{p_{\text{CO}_2\text{,FE}}}{p_{\text{ref}}}\right)^d\right]^{-1} \tag{7}$$

$$\gamma_{\text{AE}} = \frac{\tilde{R}T}{2FB_{\text{AE}}} \cdot \left[\left(\frac{p_{\text{O}_2\text{,AE}}}{p_{\text{ref}}}\right)^m\right]^{-1} \tag{8}$$

Based on the Nernst-Equation and Fickt's law of gas diffusion, the gas diffusion losses $\eta_{\text{diff},EL}$ can be derived [28] and described by Equations (9) and (10). A conversion factor $P_{\text{corr}} = 101,330$ Pa atm^{-1} is needed as well as the thickness of the gas diffusion layer L_{EL}, the microstructure parameter Ψ_{EL} at each electrode side and D_i the gas diffusion coefficient of the species i. The model Equations shown so far have been proven sufficient in order to describe cells exhibiting a Ni/YSZ FE. Extensions of these Equations have been discussed [22].

$$\eta_{\text{diff,FE}} = \frac{\tilde{R}T}{2F}\ln\left(\frac{1 + \frac{\tilde{R}TL_{\text{FE}}}{2F\Psi_{\text{FE}}D_{\text{CO}_2}p_{\text{CO}_2\text{,FE}}P_{\text{corr}}} \cdot j}{1 - \frac{\tilde{R}TL_{\text{FE}}}{2F\Psi_{\text{FE}}D_{\text{CO}}p_{\text{CO,FE}}P_{\text{corr}}} \cdot j}\right) \tag{9}$$

$$\eta_{\text{diff,AE}} = \frac{\tilde{R}T}{4F}\ln\left(\frac{1}{1 - \frac{\tilde{R}TL_{\text{AE}}\left(1-p_{\text{O}_2\text{,AE}}/p\right)}{4F\Psi_{\text{AE}}D_{\text{O}_2}p_{\text{O}_2\text{,AE}}P_{\text{corr}}} \cdot j}\right) \tag{10}$$

The microstructure parameter Ψ_{FE} and the gas diffusion layer L_{FE} at the FE are summarized as an effective gas diffusion parameter $G_{\text{eff,FE}}$ [22] in Equation (11).

$$G_{\text{eff,FE}} = \frac{\Psi_{\text{FE}}}{L_{\text{FE}}} \tag{11}$$

2.2 | Materials and methods

In this contribution, planar ESCs with a Ni/CGO FE, a 3 mol.% yttria-stabilized zirconia (3YSZ) electrolyte substrate, and a $La_w\ Sr_x\ Co_y\ Fe_z\ O_{(3-\delta)}$ (LSCF) AE were

investigated. To avoid interdiffusion, CGO layers are placed between electrodes and electrolytes [29–31]. By scanning electron microscopy the thickness of the different layers was identified for the FE of approximately 24 μm, for the electrolyte of approx. 85 μm and for the AE of approx. 30 μm. Further details on the cell and the electrode microstructure can be found [22].

The experimental cells tested in this work are schematically shown [22]. With an active cell area of 1 cm^2 for full and symmetrical cells, lateral gradients of temperature and gas conversion can be neglected. Experiments were carried out in test benches and with testing, approaches described [32] with a total flow rate of 250 sccm at each electrode side. Individual fuel and oxidant gas mixtures are set via a gas mixing unit with mass flow controllers. In an upstream combustion chamber inside the test bench, H_2O can be generated by mixing H_2 and O_2 enabling up to 100% H_2O at the fuel gas side.

The electrochemical characterization of the cell was realized by current-voltage (IV)-characteristics and impedance spectroscopy. The impedance spectra were acquired by using a pseudo-potentiostatic mode (amplitude $\leq$ 12 mV regarding the polarization resistance [32]) with a Solartron 1260 frequency response analyzer. The frequency was varied between 30 mHz and 1 MHz with 12 points per decade. Also, the spectra were commonly measured under open circuit conditions (OCV), only for the determination of the charge transfer coefficient measurements under load are required [7]. The validity of the measured spectra was verified by a "Kramers Kronig Test" [33].

Impedance spectra and IV characteristics were measured in a temperature range from 650 to 900°C. At each temperature variations of oxidant and fuel composition were performed. A summary of the operating conditions in order to parametrize the FE under CO/CO_2 conditions is given in Table A1 in the appendix. The ESC has been analyzed to deconvolute and quantify loss mechanisms by electrochemical impedance spectroscopy and the subsequent analysis of the distribution of relaxation times (DRT) [7, 12, 34]. At first, processes at fuel and AE were separated by using symmetrical cells [35, 36]. Afterwards, an overlap of gas diffusion and activation polarization as reported in [35, 37–41] at the Ni/CGO FE in the spectra was deconvoluted by using ternary fuel mixtures with high contents of inert gases such as nitrogen (N_2) and helium (He), respectively. However, [22] this can be done at a comparably high temperature of 850°C with a fuel gas mixture of $p_{H_2,FE} = 0.1$ atm and $p_{H_2O,FE} = 0.05$ atm balanced with the inert component N_2 or He, respectively, and likewise with $p_{CO,FE} = 0.1$ atm and $p_{CO_2,FE} = 0.05$ atm balanced with the inert component N_2 or He respectively. The further parametrization of the SOC becomes possible in order to develop a zero-dimensional dc model predicting the cell performance [7, 12–14, 42]. In this work, we apply an adapted approach for CO/CO_2 fuels [15, 43, 44] since the thermodynamic stability of CO/CO_2 fuel mixtures needs to be considered with respect to carbon formation.

In comparison to H_2/H_2O, CO/CO_2 fuels might form solid carbon that will be deposited in the FE and affect its performance and integrity. The thermodynamic stability of the applied CO/CO_2 fuel gas mixtures was verified by the open-source program Cantera [45] and the voltage cap in electrolysis mode was set to 1.2 V in order to prevent carbon formation. Regarding the fuel cell mode, the voltage cap was set to 0.6 V to avoid re-oxidation of Nickel in the FE [32].

In published literature [46–50] the contamination of CO_2 with, for example, sulfur impurities was found as a possible source of degradation. In the frame of this work, a stability test with different contents of CO and CO_2 has been performed without a significant degradation effect. Reference measurements at the beginning and end of the test in H_2/H_2O were conducted in order to exclude aging effects.

3 | RESULTS AND DISCUSSION

In the first step, the electrode loss mechanisms occurring at fuel and AE can be separated using symmetrical cells. The parameters in order to describe the electrochemical behavior of the LSCF AE were evaluated in a previous study [22]. Since cells from the same type are analyzed in this contribution, parameters found in a previous study [22] are assumed to remain valid for the AE of the investigated cells.

In this study fuel gas mixtures of CO/CO_2 and the related processes at the Ni/CGO FE were in focus. Fuel electrodes exhibiting a Ni/CGO FE reportedly show an overlap of electrochemical processes and gas diffusion in the spectra [35, 37–41]. In a previous study, the operation with CO/CO_2 fuel gas mixtures resulted in a shift of the gas diffusion toward lower frequencies in the spectra [51]. Figure 1 shows a DRT with a temperature variation between $T = 750$°C and $T = 900$°C of a symmetrical cell with Ni/CGO FEs with $p_{CO,FE} = 0.5$ atm (balance CO_2). All peaks in the DRT indicate a thermally activated behavior. Thus, none of the peaks can be solely related to gas diffusion, which shows a comparably low dependence on temperature ($T^{0.5}$). In the spectra, the expected contribution of the CO/CO_2 gas diffusion process is not clearly visible, which suggests that the thermally activated electrochemical process at the FE overlaps with the gas diffusion process. This overlap of several processes needs to be deconvoluted so that the activation and gas diffusion polarization processes can be quantified.

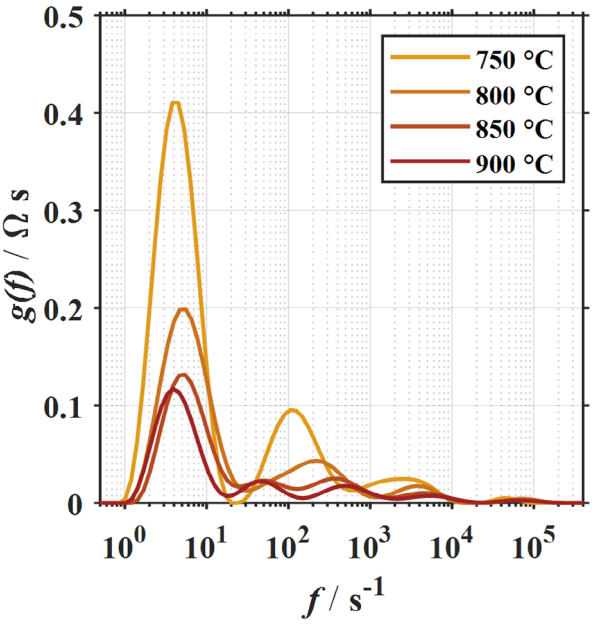

FIGURE 1 Distribution of relaxation times (DRT) with a variation of temperature of a symmetrical cell with Ni/CGO fuel electrodes with $p_{CO,FE} = 0.5$ atm (balance CO_2) between $T = 750°C$ and $T = 900°C$.

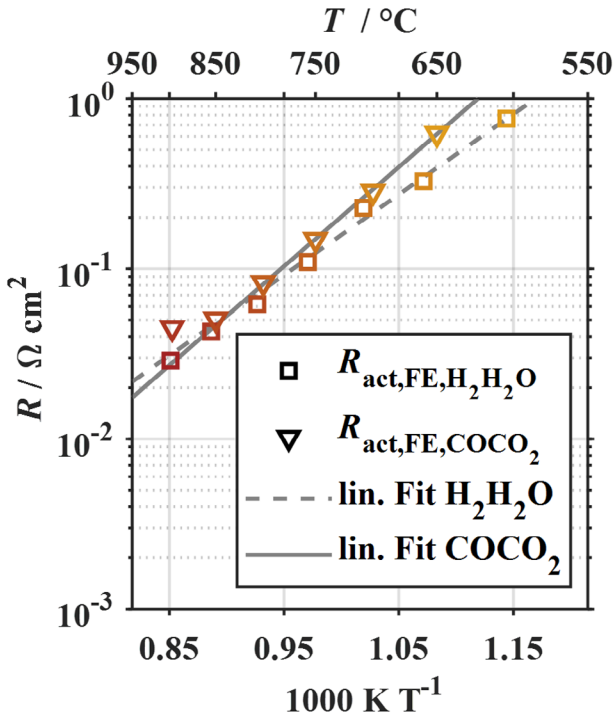

FIGURE 2 Arrhenius-plot of a temperature variation between 650 and 900°C in steps of 50°C for a gas composition with $p_{CO,FE} = 0.4$ atm (balance CO_2, triangle symbol) and between 600 and 900°C for $p_{H_2,FE} = 0.8$ atm (balance H_2O, square symbol) [22], using the area-specific resistance (ASR) values of a single electrode.

The application of ternary fuel gas mixtures with N_2 and He, respectively proved to be a suitable approach for visualizing the gas diffusion as shown for Ni/YSZ [12] and Ni/CGO FEs [39, 52, 53]. Further, a method was developed in a previous study [22] to quantify the gas diffusion process with the help of ternary fuel gas mixtures with the inert gases N_2 and He, respectively. This method shall briefly be summarized as it is described in-depth [22]. A high-accuracy test has to be performed at a rather high temperature (e.g., $T = 850°C$) as the gas diffusion resistance is proportional to $T^{0.5}$. Also, low partial pressures of the electrochemical active species (CO and CO_2) need to be chosen to enlarge the gas diffusion resistance. Electrochemical processes are assumed not to be influenced by changing the inert component in a ternary fuel mixture. Therefore, the difference in the resulting polarization resistance is purely based on gas diffusion. The latter can be used in order to determine an effective gas diffusion parameter G_{eff}. It is defined to be independent of temperature and gas compositions and therefore enables the simulation of the gas diffusion resistance [28] for individual operating conditions.

In the impedance spectra, quantifying polarization contributions with rather complex transmission line models [39, 54, 55] shall be avoided and thus, they are simply quantified by parallel connection of Ohmic resistance and constant-phase elements [22, 34]. The values of the complex non-linear least square (CNLS)-fit is divided by two accounting for one electrode. Thus, by subtracting the simulated gas diffusion resistance [28] from the measured overall polarization resistance, the activation polarization can be quantified [22]. The subsequent investigation of parameter dependencies is shown in the following.

3.1 | Activation energy fuel electrode

The area-specific resistance (ASR) values of the activation $R_{act,FE}$ are plotted as a function of temperature in Figure 2. A temperature range between 650 and 900°C in steps of 50°C for a gas composition with $p_{CO,FE} = 0.4$ atm (balance CO_2, triangle symbol) is shown. An Arrhenius behavior of the FEt's activation resistance can be observed. Therefore, the activation energy can be determined by the slope of the linear fit. Activation energy of $E_{act,FE,CO/CO_2} = 111.51$ kJ mol^{-1} (1.16 eV) was found with a cell specific constant $B_{FE,CO/CO_2} = 3.0295 \cdot 10^{-7}\ \Omega\,cm^2$. In comparison the values from the operation in H_2/H_2O mode between 600 and 900°C in steps of 50°C are presented in Figure 2 as well with $p_{H_2,FE} = 0.8$ atm (balance H_2O, square symbol). For the operation in H_2/H_2O an activation energy of $E_{act,FE,H_2/H_2O} = 90.54$ kJ mol^{-1} (0.94 eV) and a cell-specific constant of $B_{FE,H_2/H_2O} = 2.9517 \times 10^{-6}\ \Omega\,cm^2$ was extracted [22].

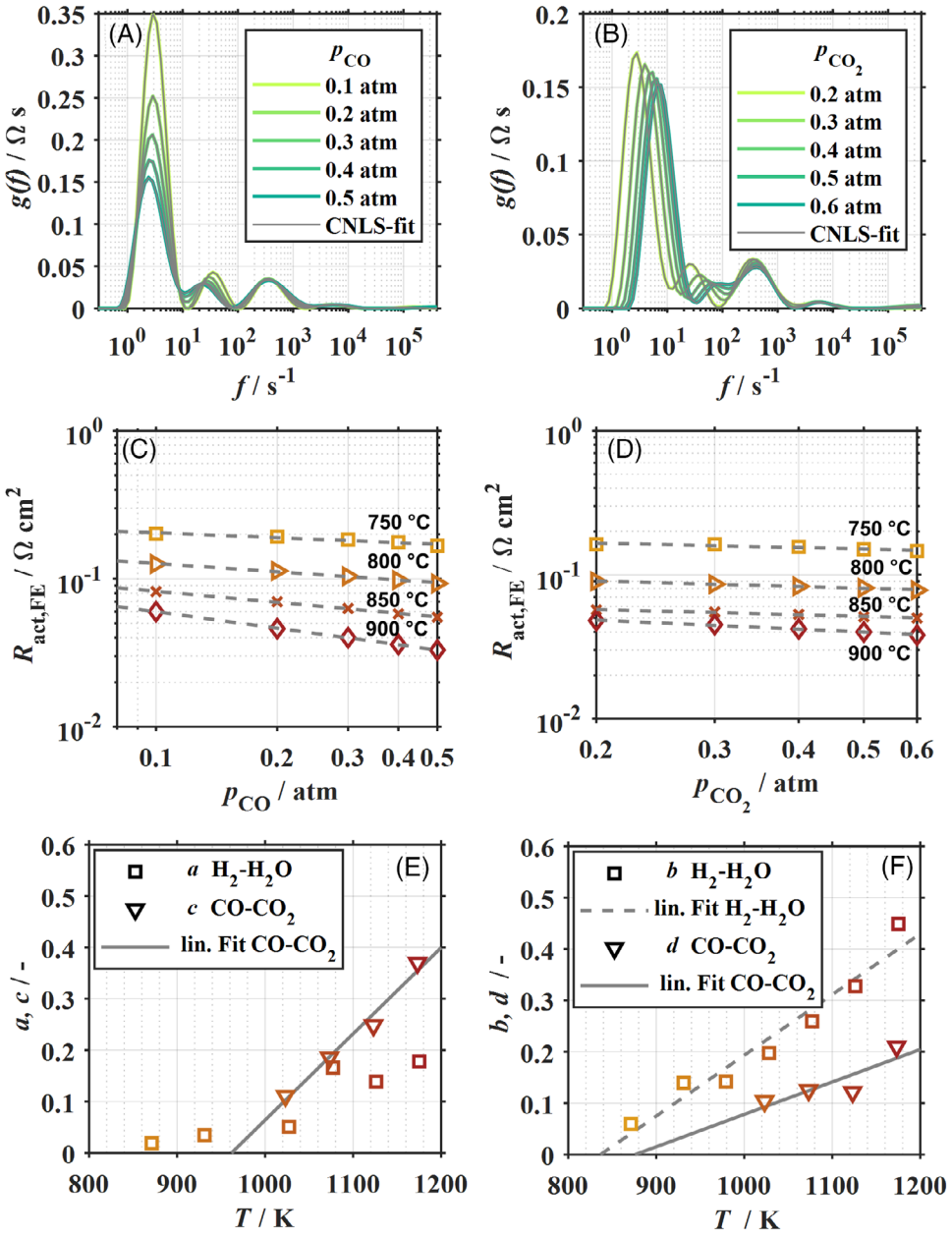

FIGURE 3 Distributions of relaxation times (DRTs) of a symmetrical cell with Ni/CGO fuel electrodes for a variation of (A) carbon monoxide partial pressure $p_{CO,FE}$ at 0.1, 0.2, 0.3, 0.4, and 0.5 atm, with a constant carbon dioxide partial pressure $p_{CO_2,FE}$ of 0.2 atm and balanced with N_2, at $T = 850°C$ and (B) a variation of the carbon dioxide partial pressure $p_{CO_2,FE}$ at 0.2, 0.3, 0.4, 0.5, and 0.6 atm with a constant $p_{CO,FE}$ of 0.4 atm and balanced with N_2, at $T = 850°C$. (C) Determination of the exponent c and (D) of the exponent d, at temperatures between 750 and 900°C using the area-specific resistance (ASR)-values of a single electrode. (E) Temperature dependency of the exponent c and (F) d for operation with CO/CO_2 and H_2/H_2O.

3.2 | Exponents *c* and *d*

The partial pressure dependency of the FEt's exchange current density toward CO and CO_2 can be described with the exponents c and d. These are determined similarly to Leonide et al. [7, 8, 15, 34] by varying one of the fuel components individually by keeping the other species on a constant level and balancing with the inert component N_2. Figure 3 shows the DRTs of a symmetrical cell with a Ni/CGO FE for a variation of (A) the carbon monoxide partial pressure $p_{CO,FE}$ at 0.1 atm, 0.2 atm, 0.3 atm, 0.4 atm, and 0.5 atm, with a constant CO_2 partial pressure $p_{CO_2,FE}$ of 0.2 atm and balanced with N_2, at $T = 850°C$ and (B) a variation of the CO_2 partial pressure $p_{CO_2,FE}$ at 0.2 atm, 0.3 atm, 0.4 atm, 0.5 atm and 0.6 atm with a constant $p_{CO,FE}$ of 0.4 atm and balanced with N_2, at $T = 850°C$. Processes at relaxation frequencies exceeding 100 Hz are hardly affected by the fuel gas composition. The

TABLE 1 Selective model parameters of the zero-dimensional cell model for the fuel electrode of the electrolyte-supported cell (ESC) with nickel/gadolinium-doped ceria (Ni/CGO) fuel electrode and the anode-supported cell (ASC) with nickel/yttria-stabilized zirconia (Ni/YSZ) fuel electrode in hydrogen/steam (H_2/H_2O) and carbon monoxide/carbon dioxide (CO/CO_2).

Parameter	Unit	ESC with Ni/CGO	ASC with Ni/YSZ
$E_{act,FE,H_2/H_2O}$	kJ mol^{-1}	90.54 [22]	105.04 [7]
$E_{act,FE,CO/CO_2}$	kJ mol^{-1}	111.51	118.64 [15]
$a(T = 600 - 750°C)$	-	0.035 [22]	−0.10 [7]
$a(T = 800 - 900°C)$	-	0.161 [22]	−0.10 [7]
$b(T)$	-	$\frac{0.0012}{K} \cdot T - 0.9892$ [22]	0.33 [7]
$c(T)$	-	$\frac{0.0017}{K} \cdot T - 1.6136$	−0.058 [15]
$d(T)$	-	$\frac{0.00063}{K} \cdot T - 0.5527$	0.25 [15]

corresponding ASR values from a single electrode resulting from the CNLS-fit are plotted as a function of the (C) CO partial pressure and (D) CO_2 partial pressure for temperatures between 750°C and 900°C in Figure 3. The exponents c and d respectively, can then be obtained by extracting the negative value of the slope of the linear fit. In agreement to H_2/H_2O atmospheres [22] a temperature dependency of the exponents can be observed in Figure 3E,F for CO/CO_2 mode as well. By a linear approximation, Equations (12) and (13) describe the temperature dependency of $c(T)$ and $d(T)$, respectively, with K as the unit Kelvin.

$$c\,(T) = \frac{0.0017}{K} \cdot T - 1.6136 \tag{12}$$

$$d\,(T) = \frac{0.00063}{K} \cdot T - 0.5527 \tag{13}$$

3.3 | Ohmic losses

The area-specific ohmic resistance $R_{ohm}(T)$ needs to be analyzed for a full cell by the thermal behavior. Similarly, the approach [22] examining the ohmic activation energy and cell-specific constant was applied. The equations with polynomial coefficients are displayed in Table A2 in the Appendix. In comparison to the parameters [22], different polynomial coefficients were found. The cells tested for H_2/H_2O and CO/CO_2 originate from the same type and were tested in the same test bench. Nevertheless, small deviations in the electrolyte thickness as well as operating temperature might result in a rather small discrepancy in the ohmic losses.

3.4 | Model parameters

Table 1 represents selective model parameters related to the FE of the ESC with Ni/CGO FE investigated here and an ASC with Ni/YSZ FE in H_2/H_2O and CO/CO_2 mode respectively [15, 22, 56, 57].

Further, the full parameter set required for modeling the IV behavior in a zero-dimensional dc performance model for CO/CO_2 fuel gas mixtures is listed in the Appendix in Table A2. No changes in the model were necessary in comparison to the methods applied for the parametrization in H_2/H_2O operation [22]. With respect to parameters not shown here (e.g., charge transfer coefficients: $\alpha_{FE,SOEC} = 0.67$ and $\alpha_{FE,SOFC} = 0.42$), no significant changes were found in comparison to [22]. Parameters for the ASC in H_2/H_2O and CO/CO_2 mode were determined [7, 8, 15, 56, 57].

3.5 | Model validation

In Figure 4, measured and simulated (continuous line) IV-curves are shown in a temperature range between T = 700°C and T = 900°C with different gas compositions of 0.3 atm CO (A) and 0.5 atm CO (B) (balance CO_2) with synthetic air at the AE. A voltage range of 600 to 1200 mV is covered. The model represents an excellent agreement with the experimentally measured IV curves (deviation of less than 4%). Considering that the actual model is isothermal and does not consider self-heating effects and the relevant parameters are obtained at OCV, the slightly higher/lower predicted voltages in the solid oxide electrolyzer cell- and solid oxide fuel cell-mode, respectively, are to be expected [42].

3.6 | Simulation studies

This approach enables a differentiated investigation of the individual loss mechanisms [8, 12, 15]. For the operation with a fuel mixture of 0.5 atm CO (balance CO_2) and synthetic air at the AE at T = 850°C the simulated absolute values of the ohmic losses η_{ohm}, activation $\eta_{act,FE}$ as

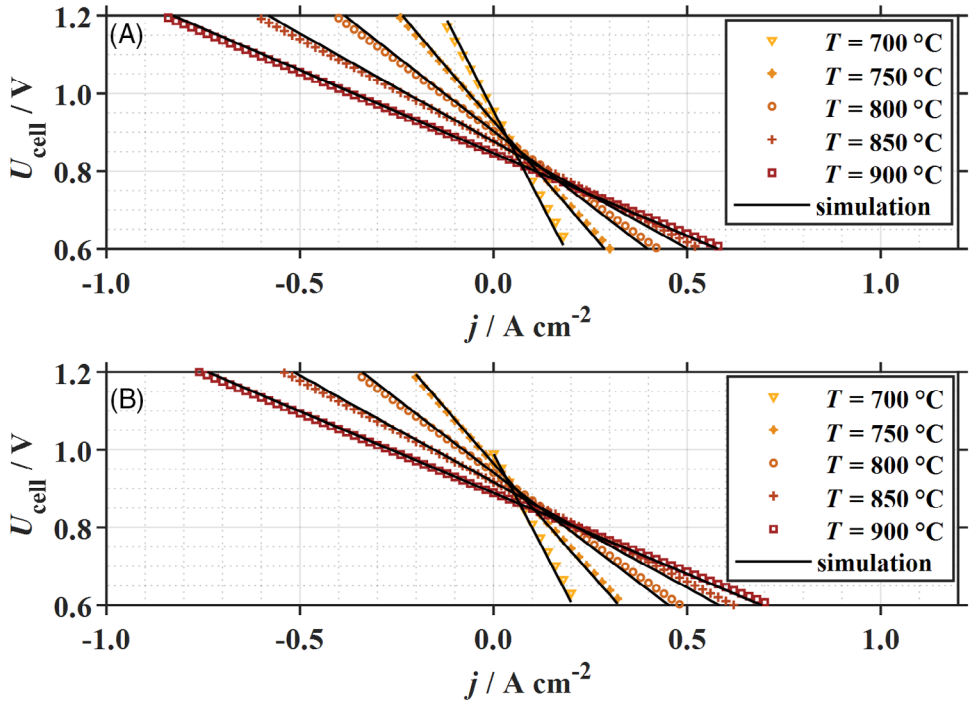

FIGURE 4 Variation of temperature between $T = 700°C$ and $T = 900°C$ with experimental and simulated (continuous line) IV-curves in solid oxide electrolyzer cell (SOEC) as well as solid oxide fuel cell (SOFC) mode with a fuel gas mixture of (A) 0.3 atm CO and (B) 0.5 atm CO (balance CO_2) with synthetic air at the air electrode.

well as gas diffusion losses $\eta_{diff,FE}$ are shown in Figure 5 as a function of the current density. The ohmic losses remain dominant as expected for an ESC. The largest relative difference between CO/CO_2 and H_2/H_2O mode can be observed for the gas diffusion losses since CO and CO_2 molecules exhibit a comparably lower gas diffusion coefficient. Anyhow, as the electrode thickness of the investigated ESCs is rather low, the overall gas diffusion losses are below ohmic and activation losses, which might be different for FE-supported cells. Visible differences in the ohmic losses were already discussed above.

The deviations between the two atmospheres become more obvious by subtracting the losses for activation and gas diffusion losses for H_2/H_2O from the corresponding losses for CO/CO_2 operation in Figure 6.

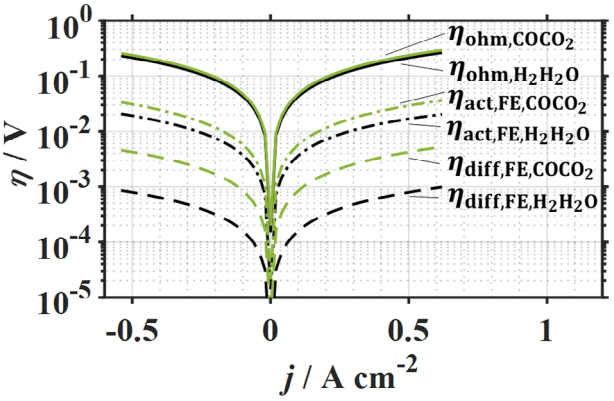

FIGURE 5 Simulated absolute values of the ohmic η_{ohm}, gas diffusion $\eta_{diff,FE}$ and activation overpotentials $\eta_{act,FE}$ in electrolyzer and fuel cell mode for the operation with 0.5 atm CO (balance CO_2) as well as 0.5 atm H_2 (balance H_2O) with synthetic air at the air electrode at $T = 850°C$.

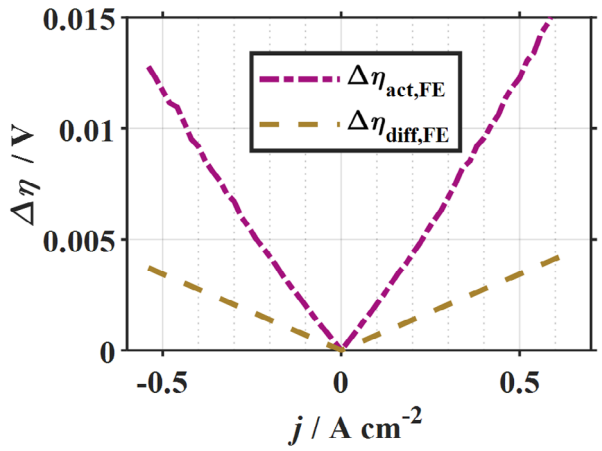

FIGURE 6 Difference of the simulated absolute values of gas diffusion $\Delta\eta_{diff,FE}$ and activation overpotentials $\Delta\eta_{act,FE}$ in electrolyzer and fuel cell mode for the operation with 0.5 atm CO (balance CO_2) as well as 0.5 atm H_2 (balance H_2O) with synthetic air at the air electrode at $T = 850°C$.

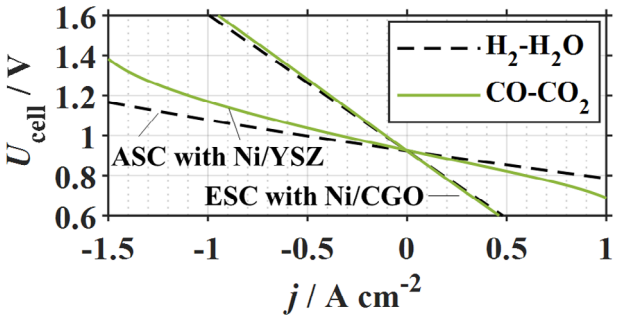

FIGURE 7 Simulated current-voltage (IV)-curves of an anode-supported cell (ASC) with nickel/yttria-stabilized zirconia (Ni/YSZ) fuel electrode and electrolyte-supported cell (ESC) with nickel/gadolinium-doped ceria (Ni/CGO) fuel electrode with 0.4 atm H_2 (balance H_2O, dashed line) and 0.4 atm CO (balance CO_2) and air at the air electrode at $T = 800°C$.

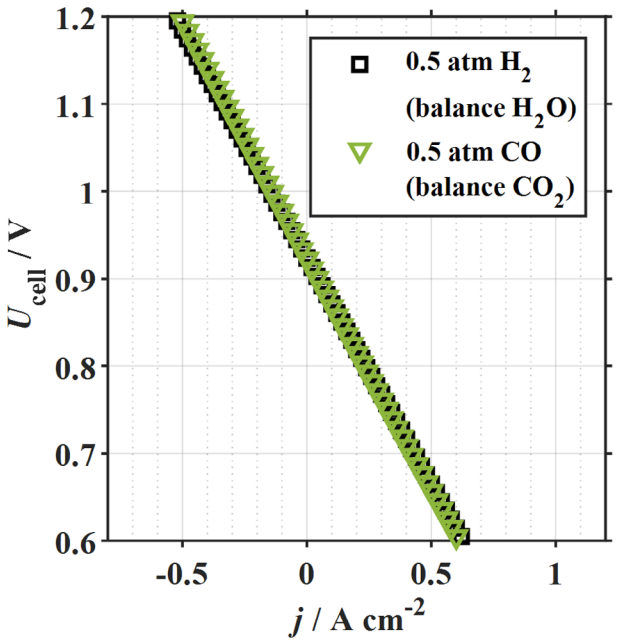

FIGURE 8 Measured current-voltage characteristics in electrolyzer and fuel cell mode for the operation with 0.5 atm H_2 (balance H_2O) as well as 0.5 atm CO (balance CO_2) and air at the air electrode at $T = 850°C$.

In Figure 7 simulated IV-curves of an ASC with Ni/YSZ FE [15] and the ESC with Ni/CGO FE investigated in this study are compared for 0.4 atm H_2 (balance H_2O, dashed line) and 0.4 atm CO (balance CO_2) at $T = 800°C$. Whereas there is only a minor difference between H_2/H_2O and CO/CO_2 fuel for the ESC with Ni/CGO FE, a larger impact becomes visible for the ASC with Ni/YSZ FE. Especially for higher current densities a significantly higher performance loss is visible for the CO/CO_2 fuel. This is related to higher gas diffusion losses as a result of the 1 mm thick porous FE substrate of the FE-supported cell [15]. In the case of CO_2-electrolysis the gas diffusion results in a gradient in CO-ratio towards the anode functional layer. At -1.5 A cm^{-2} and 1.38 V the CO-ratio increases from 0.4 atm in the gas channel to 0.92 atm in the electrochemically active functional layer. The higher CO-ratio leads to the formation of approx. 2.8 mol.% carbon based on a thermodynamic calculation in Cantera [45]. The ESC shows a less pronounced influence when operating on CO/CO_2 fuel mixtures.

3.7 | IV characteristics of H_2/H_2O and CO/CO_2

The comparison of the performance between H_2/H_2O and CO/CO_2 mode shall further be illustrated in Figure 8 for an ESC with Ni/CGO FE by measured IV-curves with 0.5 atm H_2 (balance H_2O) as well as 0.5 atm CO (balance CO_2) and air at the AE at $T = 850°C$ subsequently. The electrochemical conversion of CO/CO_2 seems to perform on a similar level as for H_2/H_2O. Further, the abovementioned discussed differences in activation and gas diffusion polarization still do not have a major impact compared to the ohmic losses regarding this cell design.

The comparison of the behavior of the fuel gas mixtures H_2/H_2O to CO/CO_2 separately delivers a basis for further investigations of reformate gas mixtures [23, 24]. In there, the water-gas-shift reaction needs to be considered as well as reforming reactions. In addition, further analysis as shown for an ASC with Ni/YSZ FE by Kromp et al. [23] was performed by Esau et al. [58] in order to judge if CO/CO_2 behaves electrochemically active in the presence of H_2/H_2O.

4 | CONCLUSIONS

A zero-dimensional impedance-based performance model for an electrolyte-supported cell with a Ni/CGO FE was extended from H_2/H_2O to CO/CO_2 fuel gas mixtures. Simulated IV curves show an excellent agreement with measurements over a wide temperature range and different gas compositions in fuel cell and electrolyzer mode. The individual loss contributions were quantified for CO/CO_2 operation. In comparison to H_2/H_2O mode, gas diffusion and activation losses become just slightly larger for CO/CO_2 operation. Nevertheless, IV-curves for the electrolyte-supported cell with Ni/CGO FE with H_2/H_2O and equivalent mixtures of CO/CO_2 show a quite similar performance as the ohmic losses remain dominant.

ACKNOWLEDGMENTS

The authors gratefully acknowledge funding from the Helmholtz project "Solar Hydrogen" and from the Federal Ministry of Education and Research (BMBF 03HY124C). Sincere thanks are given to Kerafol GmbH for providing the electrolyte substrates as well as to Sunfire GmbH for producing the cells.

Open access funding enabled and organized by Projekt DEAL.

ORCID

Cedric Grosselindemann https://orcid.org/0000-0002-9965-843X
Felix Kullmann https://orcid.org/0000-0002-6653-5601
André Weber https://orcid.org/0000-0003-1744-3732

REFERENCES

1. M. Ivanova, R. Peters, M. Müller, S. Haas, M. F. Seidler, G. Mutschke, K. Eckert, P. Röse, S. Calnan, R. Bagacki, R. Schlatmann, C. Grosselindemann, L.-A. Schäfer, N. H. Menzler, A. Weber, R. van de Krol, F. Liang, F. F. Abdi, S. Brendelberger, N. Neumann, et al. *Angew. Chem. Int. ed.* **2023**, e202218850.
2. A. Weber, *Fuel Cells* **2021**, *21*, 440.
3. A. Kromp, H. Geisler, A. Weber, E. Ivers-Tiffée. *Electrochim. Acta* **2013**, *106*, 418.
4. M. Kishimoto, H. Muroyama, S. Suzuki, M. Saito, T. Koide, Y. Takahashi, T. Horiuchi, H. Yamasaki, S. Matsumoto, H. Kubo, N. Takahashi, A. Okabe, S. Ueguchi, M. Jun, A. Tateno, T. Matsuo, T. Matsui, H. Iwai, H. Yoshida, K. Eguchi, *Fuel Cells* **2020**, *20*, 80.
5. D. M. Bierschenk, M. R. Pillai, Y. Lin, S. A. Barnett, *Fuel Cells* **2010**, *10*, 1129.
6. T. Okanishi, K. Okura, A. Srifa, H. Muroyama, T. Matsui, M. Kishimoto, M. Saito, H. Iwai, H. Yoshida, M. Saito, T. Koide, H. Iwai, S. Suzuki, Y. Takahashi, T. Horiuchi, H. Yamasaki, S. Matsumoto, S. Yumoto, H. Kubo, J. Kawahara, A. Okabe, Y. Kikkawa, T. Isomura, K. Eguchi, *Fuel Cells* **2017**, *17*, 383.
7. A. Leonide, Y. Apel, E. Ivers-Tiffée, *ECS Trans.* **2009**, *19*, 81.
8. J.-C. Njodzefon, D. Klotz, A. Kromp, A. Weber, E. Ivers-Tiffée, *J. Electrochem. Soc.* **2013**, *160*, F313.
9. L. Wehrle, Y. Wang, P. Boldrin, N. P. Brandon, O. Deutschmann, A. Banerjee, *ACS Environ. Au* **2022**, *2*, 42.
10. R. T. Leah, N. P. Brandon, P. Aguiar, *J. Power Sources* **2005**, *145*, 336.
11. O. B. Rizvandi, S. H. Jensen, H. L. Frandsen, *J. Power Sources* **2022**, *523*, 231048.
12. V. Sonn, A. Leonide, E. Ivers-Tiffée, *J. Electrochem. Soc.* **2008**, *155*, B675.
13. H. Schichlein, A. C. Müller, M. Voigts, A. Krügel, E. Ivers-Tiffée, *J. Appl. Electrochem.* **2002**, *32*, 875.
14. A. Kromp, J. Nielsen, P. Blennow, T. Klemensø, A. Weber, *Fuel Cells* **2013**, *13*, 598.
15. A. Leonide, S. Hansmann, A. Weber, E. Ivers-Tiffée, *J. Power Sources* **2011**, *196*, 7343.
16. N. Russner, S. Dierickx, A. Weber, R. Reimert, E. Ivers-Tiffée, *J. Power Sources* **2020**, *451*, 227552.
17. G. Narasimhaiah, V. M. Janardhanan, *J. Solid State Electrochem* **2013**, *17*, 2361.
18. R. Küngas, P. Blennow, T. Heiredal-Clausen, T. Holt, J. Rass-Hansen, S. Primdahl, J. Bøgild Hansen, *ECS Trans.* **2017**, *78*, 2879.
19. P. Blennow, T. Heiredal-Clausen, J. Rass-Hansen, M. Hultqvist, J. Bøgild Hansen, P. G. Moses, in *Proc. 15th Eur SOFC SOE Forum* (Eds: J. Mougin, J. Laurencin), Lucerne, Switzerland **2022**, A0304.
20. eCOs^{TM}. **2023**. can be found under, https://www.topsoe.com/our-resources/knowledge/our-products/equipment/ecos-co-from-co2
21. J. A. Hoffman, M. H. Hecht, D. Rapp, J. J. Hartvigsen, J. G. SooHoo, A. M. Aboobaker, J. B. McClean, A. M. Liu, E. D. Hinterman, M. Nasr, S. Hariharan, K. J. Horn, F. E. Meyen, H. Okkels, P. Steen, S. Elangovan, C. R. Graves, P. Khopkar, M. B. Madsen, G. E. Voecks, P. H. Smith, T. L. Skafte, K. R. Araghi, D. J. Eisenman, *Sci. Adv.* **2022**, *8*, eabp8636.
22. C. Grosselindemann, N. Russner, S. Dierickx, F. Wankmüller, A. Weber, *J. Electrochem. Soc.* **2021**, *168*, 124506.
23. A. Kromp, A. Leonide, A. Weber, E. Ivers-Tiffée, *J. Electrochem. Soc.* **2011**, *158*, B980.
24. H. Timmermann, D. Fouquet, A. Weber, E. Ivers-Tiffée, U. Hennings, R. Reimert, *Fuel Cells* **2006**, *6*, 307.
25. E. Ivers-Tiffée, H. Timmermann, A. Leonide, N. H. Menzler, J. Malzbender. in *Handbook of Fuel Cells* (Eds: W. Vielstich, A. Lamm, H.A. Gasteiger, H. Yokokawa), John Wiley & Sons, Ltd, Hoboken, NJ **2010**.
26. M. Chen, J. V. T. Høgh, J. U. Nielsen, J. J. Bentzen, S. D. Ebbesen, P. V. Hendriksen, *Fuel Cells* **2013**, *13*, 638.
27. S. B. Beale, M. Andersson, C. Boigues-Muñoz, H. L. Frandsen, Z. Lin, S. J. McPhail, M. Ni, B. Sundén, A. Weber, A. Z. Weber, *Prog. Energy Combust. Sci.* **2021**, *85*, 100902.
28. S. Primdahl, M. Mogensen, *J. Electrochem. Soc.* **1999**, *146*, 2827.
29. J. Szász, F. Wankmüller, V. Wilde, H. Störmer, D. Gerthsen, N. H. Menzler, E. Ivers-Tiffée, *J. Electrochem. Soc.* **2018**, *165*, F898.
30. A. Mai, V. A. C. Haanappel, S. Uhlenbruck, F. Tietz, D. Stöver, *Solid State Ionics* **2005**, *176*, 1341.
31. A. Mai, V. A. C. Haanappel, F. Tietz, D. Stöver, *Solid State Ionics* **2006**, *177*, 2103.
32. D. Klotz, A. Weber, E. Ivers-Tiffée, *Electrochim. Acta* **2017**, *227*, 110.
33. M. Schönleber, D. Klotz, E. Ivers-Tiffée, *Electrochim. Acta* **2014**, *131*, 20.
34. A. Leonide, V. Sonn, A. Weber, E. Ivers-Tiffée, *J Electrochem. Soc.* **2008**, *155*, B36.
35. M. Riegraf, R. Costa, G. Schiller, K. A. Friedrich, S. Dierickx, A. Weber, *J. Electrochem. Soc.* **2019**, *166*, F865.
36. J. R. Mulligan, S. Gopalan, U. B. Pal, S. N. Basu, *JOM* **2022**, *74*, 4527.
37. M. Riegraf, V. Yurkiv, R. Costa, G. Schiller, K. A. Friedrich, *ChemSusChem* **2017**, *10*, 587.
38. V. A. Rojek-Wöckner, A. K. Opitz, M. Brandner, J. Mathé, M. Bram, *J. Power Sources* **2016**, *328*, 65.
39. A. Nenning, C. Bischof, J. Fleig, M. Bram, A. K. Opitz, *Energies* **2020**, *13*, 987.

40. A. Weber, S. Dierickx, N. Russner, E. Ivers-Tiffée, *ECS Trans.* **2017**, *77*, 141.
41. A. Hagen, A. K. Padinjarethil, J. Heijne, *Electrochim. Acta* **2023**, *461*, 142672.
42. D. Klotz, A. Leonide, A. Weber, E. Ivers-Tiffée, *Int. J. Hydrogen Energy* **2014**, *39*, 20844.
43. Y. Song, X. Zhang, K. Xie, G. Wang, X. Bao, *Adv. Mater.* **2019**, *31*, 1902033.
44. R. Küngas, *J. Electrochem Soc.* **2020**, *167*, 044508.
45. Cantera. **2022**. can be found under, https://www.cantera.org,
46. S. D. Ebbesen, M. Mogensen, *Electrochem. Solid-State Lett.* **2010**, *13*, B106.
47. C. Graves, S. D. Ebbesen, M. Mogensen, *Solid State Ionics* **2011**, *192*, 398.
48. A. Hauch, M. L. Traulsen, R. Küngas, T. L. Skafte, *J. Power Sources* **2021**, *506*, 230108.
49. S. D. Ebbesen, M. Mogensen, *J. Power Sources* **2009**, *193*, 349.
50. M. Riegraf, K. Develos-Bagarinao, I. Biswas, R. Costa, *J. Power Sources* **2023**, *559*, 232669.
51. C. Endler, A. Leonide, A. Weber, F. Tietz, E. Ivers-Tiffée, *J. Electrochem. Soc.* **2010**, *157*, B292.
52. P. V. Aravind, J. P. Ouweltjes, J. Schoonman, *J. Electrochem Soc* **2009**, *156*, B1417.
53. A. Mohammed Hussain, J. V. T. Høgh, T. Jacobsen, N. Bonanos, *Int. J. Hydrogen Energy* **2012**, *37*, 4309.
54. S. Dierickx, T. Mundloch, A. Weber, E. Ivers-Tiffée, *J. Power Sources* **2019**, *415*, 69.
55. A. Weber, *TM Tech. Mess.* **2020**, *88*, 1.
56. A. Leonide, *Ph.D. Thesis*, Karlsruhe Institute of Technology (Germany) **2010**.
57. J.-C. Njodzefon, *Ph.D. Thesis* Technical University of Denmark **2015**.
58. D. Esau, C. Grosselindemann, S. P. Sckuhr, F. Kullmann, L. Wissmeier, A. Weber, *ECS Trans.* **2023**, *111*, 871.

How to cite this article: C. Grosselindemann, F. Kullmann, T. Lehnert, O. Fritz, F. M. Fuchs, A. Weber, *Fuel Cells* **2023**, 1.
https://doi.org/10.1002/fuce.202300060

A. APPENDIX

TABLE A1 Operating conditions of impedance measurements for parametrization of the fuel electrode under carbon monoxide/carbon dioxide (CO/CO_2) mode.

Parameter	Operating conditions
$E_{act,ohm}$	Full cell; $T = 700 - 900°C$ (50°C steps); $p_{CO,FE} = 0.4$ atm (balance CO_2); synthetic air at the air side;
B_{ohm}	
k_1	
k_2	
k_3	
$E_{act,FE}$	Symmetrical fuel electrode; $T = 650 - 900°C$ (50°C steps); with $p_{CO,FE} = 0.4$ atm (balance CO_2)
B_{FE}	
$c(T)$	Symmetrical cell; $T = 750 - 900°C$ (50°C steps); $p_{CO,FE} = 0.1$ atm, 0.2 atm, 0.3 atm, 0.4 atm, and 0.5 atm, with a constant carbon dioxide partial pressure $p_{CO_2,FE}$ of 0.2 atm and balanced with N_2;
$d(T)$	Symmetrical cell; $T = 750 - 900°C$ (50°C steps); $p_{CO_2,FE} = 0.2$ atm, 0.3 atm, 0.4 atm, 0.5 atm and 0.6 atm with a constant $p_{CO,FE}$ of 0.4 atm and balanced with N_2;
$\alpha_{FE,SOEC}$	Full cell; $T = 750°C$; $p_{CO,FE} = 0.38$ atm (balance CO_2); synthetic air at the air side; $\lvert j \rvert = 0.05 - 0.25$ A cm^{-2} (steps of $\lvert j \rvert = 0.05$ A cm^{-2})
$\alpha_{FE,SOFC}$	
G_{eff} [22]	Symmetrical fuel electrode; $T = 850°C$; $p_{H_2,FE} = 0.1$ atm and $p_{H_2O,FE} = 0.05$ atm balanced with the inert component N_2 or He respectively;

TABLE A2 Model parameters of the zero-dimensional cell model adapted to a solid oxide cell with nickel/gadolinium-doped ceria (Ni/CGO) fuel electrode, 3 mol.% yttria-stabilized zirconia (3YSZ) electrolyte and $La_w\ Sr_x\ Co_y\ Fe_z\ O_{(3-\delta)}$ (LSCF) air electrode for operation in carbon monoxide/carbon dioxide (CO/CO_2).

Parameter	Unit	Value
$E_{\mathrm{act,ohm}}$	$\mathrm{J\ mol^{-1}}$	$1000\ \mathrm{K} \cdot \tilde{R}\,(2\,k_1\,x + k_2 + \frac{1}{x})$ with $x = \frac{1000\ \mathrm{K}}{T}$ [22]
B_{ohm}	$\mathrm{K\ \Omega^{-1}\ m^{-2}}$	$\frac{1000\ \mathrm{K}}{x}\frac{10^4}{\Omega\ \mathrm{m^2}} \cdot \exp(-(k_1\,x^2 + k_2\,x + k_3 - \frac{E_{\mathrm{act,ohm}}}{1000\ \mathrm{K}\cdot\tilde{R}} \cdot x))$ [22]
k_1	-	13.2739
k_2	-	−16.643
k_3	-	3.5519
$E_{\mathrm{act,FE}}$	$\mathrm{kJ\ mol^{-1}}$	111.51
B_{FE}	$\Omega\ \mathrm{m^2}$	$3.0295 \cdot 10^{-11}$
$c(T)$	-	$\frac{0.0017}{\mathrm{K}} \cdot T - 1.6136$
$d(T)$	-	$\frac{0.00063}{\mathrm{K}} \cdot T - 0.5527$
$\gamma_{\mathrm{FE}}(T)$	$\mathrm{A\ m^{-2}}$	$1.42 \times 10^6\ (\mathrm{A\ m^{-2}\ K^{-1}}) \cdot [0.4^{c(T)} \cdot 0.6^{d(T)}]^{-1} \cdot T$
$\alpha_{\mathrm{FE,SOEC}}$	-	0.67
$\alpha_{\mathrm{FE,SOFC}}$	-	0.42
G_{eff}	$\mathrm{m^{-1}}$	736.87 [22]
$E_{\mathrm{act,AE}}$	$\mathrm{kJ\ mol^{-1}}$	144.54 [22]
B_{AE}	$\Omega\ \mathrm{m^2}$	1.5185×10^{-14} [22]
m	-	0.42 [22]
$\gamma_{\mathrm{AE}}(T)$	$\mathrm{A\ m^{-2}}$	$5.47 \times 10^9\ (\mathrm{A\ m^{-2}\ K^{-1}}) \cdot T$ [22]
α_{AE}	-	0.65 [7]
Ψ_{AE}	-	0.048 [22]